Germanium doping of wider-band-gap $CuGaSe_2$ chalcopyrites: Local and electronic structure

V. Koteski
VINČA, University of Belgrade, P.O. Box 522, 11001 Belgrade, Serbia

S. Doka-Yamigno, J. Hofstetter, M. Rusu, H.-E. Mahnke,*,† M. Ch. Lux-Steiner,† and Th. Schedel-Niedrig
Helmholtz-Zentrum Berlin GmbH, Hahn-Meitner-Platz 1, D-14109 Berlin, Germany

E. Arushanov
Institute of Applied Physics, Academy of Sciences of the Republic Moldova, Academiei 5, Chisinau 277028, Moldova
(Received 8 October 2009; revised manuscript received 19 April 2010; published 24 June 2010)

We present here a complementary study on germanium doping of the wider-band-gap $CuGaSe_2$ (CGS) chalcopyrite. In photoluminescence studies, the occurrence of a new emission line was identified as Ge related and explained as a donor-acceptor-pair recombination. The precise role the Ge is playing in this doping of CGS is revealed by x-ray absorption spectroscopy and *ab initio* calculations based on the density-functional theory. Extended x-ray absorption fine-structure spectroscopy (EXAFS) as well as x-ray absorption near-edge spectroscopy performed at the Ge *K*-, Cu *K*-, and Ga *K*-edge show that the Ge dopants occupy the cationic sites of Ge_{Cu} or Ge_{Ga} of the host lattice. The complementary *ab initio* calculations support the EXAFS results. They further indicate that the incorporated Ge atoms preferentially occupy Ga sites when relaxation around the dopant is taken into account. Additionally, our corresponding theoretical band-structure model predicts the existence of additional localized electronic acceptor and donor defect bands within the band gap of $CuGaSe_2$ originating from a strong covalent interaction between Ge 4*s* and Se 4*p* states for Ge atoms tetrahedrally surrounded by the Se nearest-neighbor atoms. A theoretically predicted antibonding Ge-Se $4sp^3$ defect band appearing well above the Fermi level for the Ge_{Ga}^{1+} point-defect system can be directly linked to a Ge-dopant-related donor-acceptor-pair transition as observed in our photoluminescence spectra.

DOI: 10.1103/PhysRevB.81.245213 PACS number(s): 61.72.up, 61.05.cj, 71.15.Mb

I. INTRODUCTION

The wider-band-gap $CuGaSe_2$ (CGS) is a nonlinear optical I-III-VI_2 material belonging to the copper-based chalcopyrite family which is considered to be a promising class of light absorbing material used in solar-cell applications with a proven efficiency of about 20% for $Cu(In_{1-x},Ga_x)_{(x=0.25-0.35)}Se_2$.[1] However, there is still a huge difference between the reported experimental photovoltaic conversion efficiencies of ~10% and the theoretical predictions of ~25% for heterojunction solar cells based on $CuGaSe_2$ chalcopyrite semiconductor with a band gap of 1.7 eV. One way of improving the efficiency of these solar cells would be to achieve a *p*-to-*n*-type inversion at the $CuGaSe_2$/CdS heterojunction interface[2] of a standard *n*-ZnO/*i*-ZnO/*n*-CdS/*p*-$CuGaSe_2$ solar-cell device. Therefore, an extrinsic *n*-type doping of the surface/near-surface region of *p*-type $CuGaSe_2$ has become an area of interest.[3–5] The preparation of *n*-type $CuGaSe_2$ material can be achieved either by lowering the concentration of shallow acceptors such as mainly Cu vacancies, V_{Cu}, or by introducing additional defect states such as shallow donors. Doping of the ternary $CuGaSe_2$ semiconductor with group-IV elements such as C, Si, Ge, or Sn offers the possibility to force the formation of two donating point defects in the chalcopyrite lattice, Ge_{Cu} and Ge_{Ga}. Accordingly, Ge atoms were introduced into $CuGaSe_2$ semiconductors as potential candidates for donor atoms.

However, $CuGaSe_2$ chalcopyrite based solar cells have encountered many difficulties which were, in principle, explained by the doping pinning rule.[6,7] One problem encountered when incorporating Ge doping atoms into $CuGaSe_2$ could be the formation of defect complexes due to the induced lattice distortions around the impurity atoms. Thus, many attempts of extrinsic doping by means of ion implantation have been made to overcome this problem and to understand the doping mechanisms of extrinsic impurities into the $CuGaSe_2$ host lattice. These difficulties to *n*-type dope $CuGaSe_2$ are an example for the general trend that wider-band-gap members of a semiconductor series often resist *n*-type doping similar to the well-known example of diamond as a wide-band-gap material.

In this work we present the experimental evidence for a Ge-related new photoluminescence (PL) line to be ascribed to a donor-acceptor transition. X-ray absorption spectroscopy data reveal the local structure of the incorporated Ge dopants combined with theoretical calculations of the lattice relaxation around the Ge impurity atom in Ge-doped $CuGaSe_2$ using the WIEN2K package.[8] Additional results on electronic-structure calculations will be presented for different Ge-dopant point-defect arrangements and will be used to strengthen our assignments.

II. EXPERIMENTAL METHODS

$CuGaSe_2$ thin films of a thickness of about 2 μm were prepared by a chemical-vapor transport process in a close-space arrangement, named chemical close-spaced vapor transport (CCSVT) technique, on Mo-coated soda lime glass substrates under $GaCl_x/H_2Se$ atmosphere.[9] The resulting thin-film solar cells based on such thin-film $CuGaSe_2$ ab-

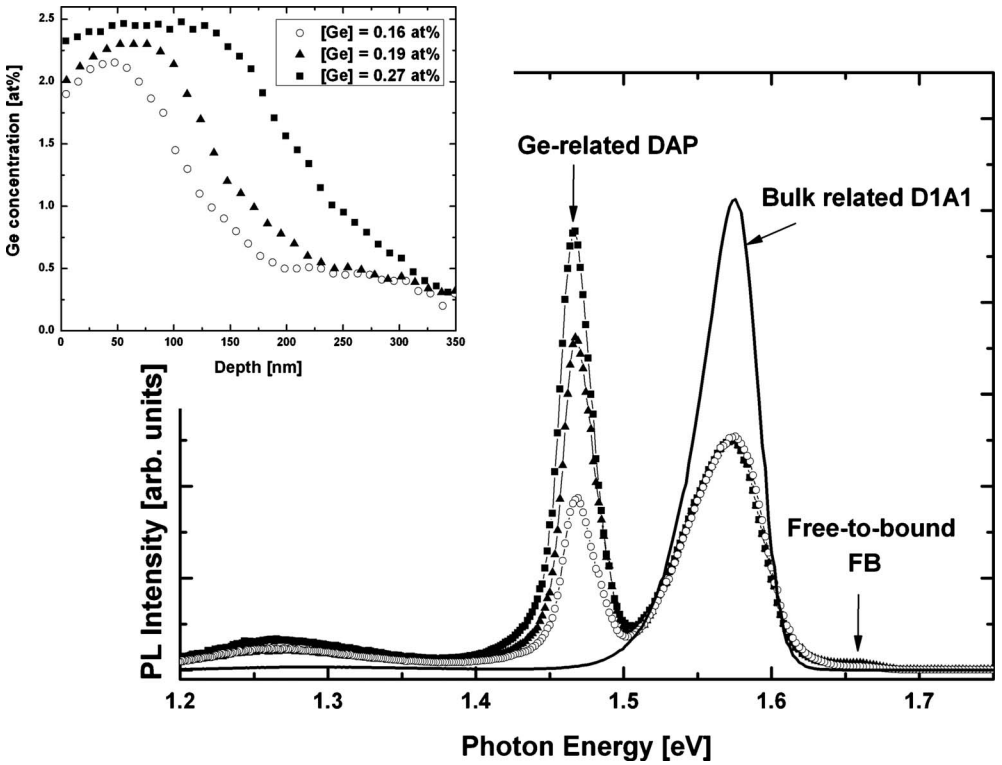

FIG. 1. Photoluminescence of as-grown (bulk) and Ge-implanted $CuGaSe_2$ thin films as a function of Ge atomic concentration as determined by SNMS and shown in the inset ($T=10$ K, $\lambda=351.1$ nm, UV excitation with a power of the laser of $P_{exc}=20$ mW). An almost constant Ge concentration of 2.0–2.5 at. % has been obtained in the implantation regions of 80, 120, and 180 nm by using three different Ge ion fluences and energies with varying Ge ion-penetration depths into the near-surface region of $CuGaSe_2$ (see inset of Fig. 1) resulting in different amounts of implanted Ge ions. Only when averaged over the whole film thickness of about 2 μm, the Ge concentration result as labeled in the insert (varying from 0.16% to 0.27%).

sorber layers show conversion efficiencies of up to 8.7% (active area).[10] We have irradiated the thin films with Ge ions with different fluences and energies in order to obtain a constant Ge concentration doping profile in the near-surface region of $CuGaSe_2$ up to a depth of 200 nm. For a defect healing caused by the implantation procedure, we applied an annealing step in vacuum ($p \approx 1 \times 10^{-5}$ mbar) at 400 °C for 15 min. At this temperature we only expect a surface oxidation of the first few nanometers to Ga_2O_3 and SeO_2 with some minor Na_2CO_3 contributions as a kind of protection layer avoiding a bulk oxidation.[11]

As determined by secondary neutral mass spectroscopy (SNMS) (see inset of Fig. 1), we measured an almost constant Ge concentration of 2.0–2.5 at. % in the resulting implantation regions of 80 nm (sample 1, irradiated with a fluence of 1×10^{16} ions/cm^2 at an energy of 50 keV), 120 nm (sample 2, irradiated with a fluence of 1×10^{16} ions/cm^2 at an energy of 150 keV), and 180 nm (sample 3, irradiated with a fluence of 3×10^{15} ions/cm^2 at an energy of 50 keV plus 7×10^{15} ions/cm^2 at an energy of 150keV and with 1×10^{16} ions/cm^2 at an energy of 200 keV). When averaged over the whole film thickness of about 2 μm, the Ge concentration would correspond to a concentration of approximately 0.3 at. % (for more details see Refs. 4, 5, and 12).

The photoluminescence measurements were carried out by using the 351.2 nm lines of an argon-ion laser as the excitation source. Samples were mounted in a helium cryostat at fixed temperature of 10 K and the power of the laser was set to 20 mW. The luminescent light was analyzed by a 0.22 m double-lattice monochromator and detected by a photomultiplier.

Besides thin films, single crystals of $CuGaSe_2$ were prepared by standard CVT from the respective elements with about 1 wt % Ge and iodine as transport agent resulting in a Ge concentration of about 0.3 at. % in the $CuGaSe_2$ single-crystalline samples as determined by energy-dispersive x-ray analysis.[12] Hence, in the present study, the homogeneous Ge concentration of 0.3 at. % in grown single-crystalline samples matches the averaged Ge concentration in the thin-film Ge-implanted material. We have used the single-crystalline material for complementary x-ray absorption experiments since the effective absorber thickness could be more easily adjusted for optimal fluorescence yields (see below).

The x-ray absorption, in the extended x-ray absorption fine structure (EXAFS) and in the x-ray absorption near-edge structure (XANES) version, was measured at the *K*-edge Ge (Cu and Ga as well) in the fluorescence yield mode at the A1 beamline of HASYLAB at DESY. The fluorescence was detected with a seven-segment Ge detector in line with the polarization vector of the incoming synchrotron radiation. The Ge-doped $CuGaSe_2$ thin films were directly mounted on a cold finger of a liquid-nitrogen cryostat. Additional samples prepared from single-crystalline material were also

measured. They were prepared as pellets made up from pressed powder of Ge-doped $CuGaSe_2$ single crystals mixed with graphite and polyethylene for a better sample stability and temperature control and to optimize the absorption length.

III. COMPUTATIONAL METHOD

Our calculations were performed within the framework of the density-functional theory employing the linearized augmented plane-wave (LAPW) method by using the code WIEN2K.[8] The structural relaxation around the Ge atom in $CuGaSe_2$ was studied also by using the WIEN2K code.[8] In the LAPW method the unit cell is divided into atom-centered muffin-tin (MT) spheres and in-between regions. The chalcopyrite crystal structure has a body-centered tetragonal (bct) Bravais lattice for which the primitive unit-cell lattice vectors can be chosen as $(a/2,a/2,-c/2)$, $(a/2,-a/2,c/2)$, and $(-a/2,a/2,c/2)$ (see Sec. IV B). After performing structural relaxation on the bct unit cell of the pure chalcopyrite $CuGaSe_2$ crystal structure which included internal degrees of freedom, volume and c/a relaxation, the thus obtained structural parameters were used to setup the defect system relaxation. The impurity system was treated by constructing a 64-atom supercell where one of the host cations was replaced by Ge. Since the supercell was constructed by using the fully relaxed conventional unit cell of $CuGaSe_2$, the relaxation procedure for the 64-atoms system was performed by moving at least four nearest-neighbor (NN) shells around the impurity according to the Hellmann-Feynman forces with a convergence criterion set to 1 mRy/a.u. (1 a.u., i.e., the Bohr radius, corresponds to 0.529×10^{-8} cm). During the relaxation, the point-group symmetry of the impurity was preserved, in agreement with the results of our experimental EXAFS fitting (see Sec. IV).

In order to achieve good energy convergence and at the same time to make our calculations computationally feasible, we expanded the basis function up to $R_{\mathrm{MT}}K_{max}=7$ (where K_{max} is the maximum modulus for the reciprocal-lattice vector and R_{MT} is the smallest MT radius). The iteration process was continued until the charge between two successive iterations was less than 0.0001 electrons. The radii of the MT spheres for Cu, Ga, Se, and Ge were chosen to be 2.33 a.u., 2.24 a.u., 2.07 a.u., and 2.29 a.u., respectively. The Brillouin zone (BZ) was sampled with 125 k points that were reduced to 12 k points in the irreducible part of the BZ. We used the generalized gradient approximation in its Perdew, Burke, and Ernzerhof parametrization.[13]

As a consequence of the local-density approximation (LDA), the band-gap energy is typically underestimated and, hence, much smaller than the corresponding experimentally determined band-gap energy of 1.68 eV for $CuGaSe_2$. Sometimes additional techniques are applied to artificially match the calculated and experimental band gaps, e.g., Ref. 14. Here we do not use such expansion methods since our main conclusions do not depend on a precise determination of the band gap.

IV. RESULTS AND DISCUSSION

A. Experimental results

Figure 1 shows the UV-excited photoluminescence spectra of the Ge-implanted $CuGaSe_2$ films recorded after the annealing process for different Ge concentrations determined by SNMS and estimated by integration within the complete film depth to be between 0.16 and 0.27 at. % as indicated in the inset of the Fig. 1. The intensity of the photoluminescence emission at 1.47 eV previously ascribed to donor-acceptor-pair (DAP) transition[4,5] is normalized to the intensity of the well-known donor-acceptor transition labeled D1A1 occurring at 1.58 eV.[5,15]

Besides the well-known DAP emission at 1.58 eV, we observe a new strong photoluminescence emission at 1.47 eV which is correlated with the Ge implantation. The new feature is assigned to a donor-to-acceptor pair recombination as determined by means of power-dependent photoluminescence spectroscopy[4] and using the power law $\boldsymbol{I}_{\mathrm{PL}}=\boldsymbol{cxP}_{exc}^{\boldsymbol{k}}$ [where $\boldsymbol{I}_{\mathrm{PL}}$ represents the photoluminescence intensity, $\boldsymbol{P}_{exc}$ the excitation power of the laser, and $\boldsymbol{c}$ a constant]. The $\boldsymbol{k}$ values of both photoluminescence emissions at 1.58 *and* 1.47 eV are 0.44 and 0.64, i.e., $\boldsymbol{k}<1$, which are characteristic for a defect-correlated recombination mechanism.[4,5,16]

The Ge doping opens a new radiative decay channel for the photoluminescence process. We found a new DAP transition in the course of the doping at 1.47 eV which is attributed to a new donor defect level in the band gap of bulk $CuGaSe_2$. Hence, *only* for the Ge-doped spectra the intensity of the well-known DAP emission in $CuGaSe_2$ appearing at 1.58 eV is set to a constant value (normalization). The absolute detected intensity of this DAP of the undoped "bulk" $CuGaSe_2$ is about a factor of 2 higher if compared to the doped $CuGaSe_2$:Ge spectrum of the second photoluminescence spectrum (filled triangles). This strongly indicates that the photoluminescence intensity of the DAP at 1.58 eV partly appears now at 1.47 eV due to a second radiative decay channel via the new donor defect level. The intensity of the Ge-related DAP at 1.47 eV depends only on the total number of implanted Ge atoms in the implantation regions of 80, 120, and 180 nm. That this scaling is not absolutely perfect is due to a "dead layer" near the surface (oxidation, loss of Ge, etc.). A possible link between the DAP to defects produced by just the implantation and not the incorporation of Ge could be ruled out by an earlier implantation of Zn under similar conditions, after which the DAP at 1.47 eV was not observed.

While the new emission line is well characterized in PL spectroscopy, the local structure of the participating Ge dopant needs to be solved as achieved by the absorption spectroscopy. The analysis of the experimental absorption spectra $\chi(k)$ was performed using the standard ATHENA/ARTEMIS code combination.[17] After performing background subtraction, the EXAFS spectra were Fourier transformed into r space, where the fitting was conducted. Two sets of theoretical fitting standards were obtained employing the FEFF8 (Ref. 18) *ab initio* multiple-scattering program on a cluster of 71 atoms of pure CGS structure: one with Ge substituting on the Ga site, $\mathrm{Ge_{Ga}}$, and the other with Ge on the Cu site, $\mathrm{Ge_{Cu}}$. Both Ge substitution models produced excellent fits with very similar R factors (fit quality factor), bond lengths, and other structural and electronic parameters, indicating that we cannot determine a Ge-dopant site preference from the EXAFS analysis alone. We also obtained virtually identical results after performing a more detailed EXAFS analysis in-

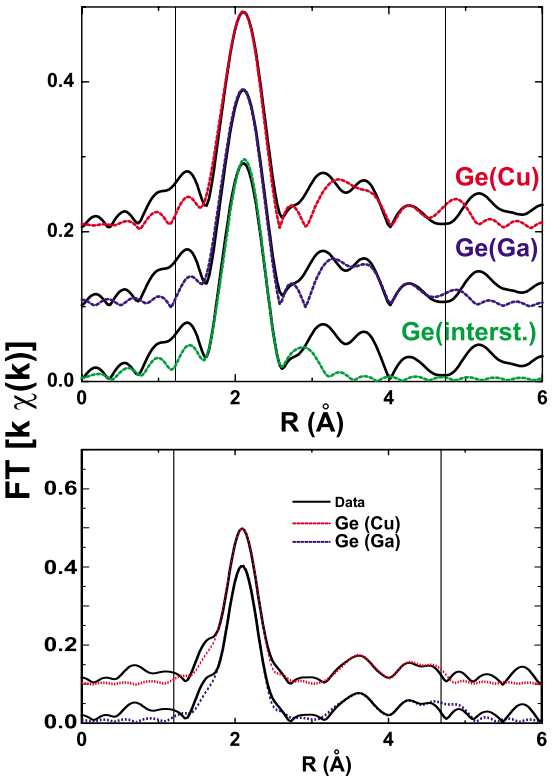

FIG. 2. (Color online) Radial distribution function, i.e., Fourier transform of the *k*-weighted EXAFS spectrum for Ge in a polycrystalline $CuGaSe_2$ film prepared by Ge implantation, as measured at 80 K (upper part) and in powdered material prepared from single-crystalline material grown by CVT (lower part). For the polycrystalline film material the experimental data are compared to three model situations: Ge on the Cu site—top spectrum, Ge on the Ga site—center spectrum, and Ge on an interstitial position, for the CVT-grown material the comparison is given only for Ge on the Cu site (upper curve) and Ge on Ga site (lower curve). The vertical lines denote the fitted region of the first three shells around Ge.

cluding structural optimization (see the next section) and using a markedly different Ge_{Ga} and Ge_{Cu} relaxed structures in order to produce the theoretical standards. This is not surprising since the first-nearest-neighbor shell of selenium atoms around the central Ge atom is identical regardless of whether Ge atoms occupy a Cu or Ga position in the host lattice and, hence, the fit naturally adjusts the distances to match the experimental data.

The difference should, in principle, be more pronounced in the second shell which is made out of three subshells: two Ga and one Cu subshell in the Ge_{Cu} and two Cu and one Ga in the Ge_{Ga} case. But these small differences have no practical influence on the fitting results which can be seen in the upper part of Fig. 2 where the radial distribution function is presented around Ge atoms in polycrystalline thin film $CuGaSe_2$. The same result was obtained for single-crystalline samples where we could obtain higher statistics due to optimized absorption thickness in the experiment, see the lower part of Fig. 2. During the fitting procedure the coordination numbers were held constant to the values in the undoped system. The fitting results show an inwardly directed relaxation of the first neighboring Se shell around a Ge dopant, and an identical Ge-Se distance of 2.40(2) Å was found (see Table I). As shown in Fig. 2, the data do not allow a distinction of the two possibilities for the cationic sublattice by the second and third shell region in *r* space, partly because of reduced statistics, but also partly very likely due to a higher degree of disorder in those shells because of higher local concentration in the film material as compared to the crystalline bulk sample.

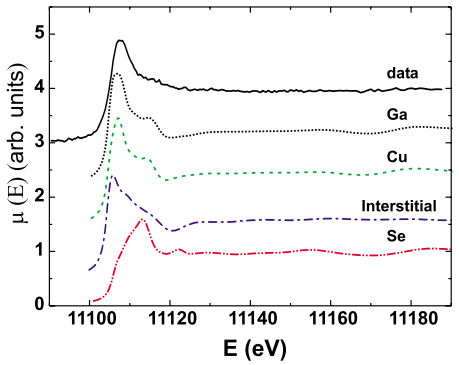

FIG. 3. (Color online) Ge *K*-XANES data of $CuGaSe_2$:Ge and the resulting full multiple-scattering calculations for the four different atomic positions of the Ge dopants in CGS, Ge_{Ga}, Ge_{Cu}, and Ge_{Se} and an adopted interstitial position at $(0.5a, 0.5b, 0.25c)$. A clear preference for an interpretation as one of the two cationic options is obviously not possible.

We have also theoretically simulated the XANES spectra (Fig. 3) at the Ge *K* edge by using the full multiple-scattering (FMS) capabilities of the FEFF computational code for both possible cationic positions of Ge, Ge_{Ga}, and Ge_{Cu}, and, in addition, also for the anionic Ge_{Se} position. The FMS was performed on a neutral cluster with 99 atoms around the central absorbing atom.

Agreement with the experimental data of the single-crystalline and polycrystalline system was observed only in the case where Ge atoms occupy the cationic sites of either

TABLE I. Fitted values from EXAFS data around Ge in the $CuGaSe_2$ thin-film material of the nearest-neighbor distance R_{NN}, mean-square displacement σ^2, energy shift ΔE, amplitude reduction factor S_0^2, and fit-quality factor *R*. (The respective values for the powdered single-crystalline material turned out to be the same, only with smaller statistical errors.)

Thin film	R_{NN} (Å)	σ^2 (Å^2)	ΔE (eV)	S_0^2	*R* factor (%)
Ge(Cu)	2.40(2)	0.003(3)	6(5)	0.8(4)	3.9
Ge(Ga)	2.40(2)	0.003(2)	5(5)	0.8(3)	3.6

TABLE II. Lattice parameters and bond lengths of $CuGaSe_2$ derived from XRD and EXAFS on the Cu *K* and Ga *K* edge, respectively.

Lattice parameters	X-ray diffraction [Ref. S. Lehmann (Ref. 18)] (T=300 K)	ICSD [Ref. ICSD (Ref. 19)] (T=300 K)	EXAFS analysis (T=100 K)
a_o (Å)	5.617(1)	5.614(1)	
c_o (Å)	11.024(1)	11.022(1)	
η	0.981(1)	0.982(1)	
u	0.257(1)	0.259(4)	
$R_{\text{Cu-Se}}$ (Å)	2.441(2)	2.447(2)	2.412(3)
$R_{\text{Ga-Se}}$ (Å)	2.394(2)	2.389(2)	2.405(3)

Ge_{Cu} (dashed line) or Ge_{Ga} (dotted line) in the host $CuGaSe_2$ lattice. Here, the characteristic features of the simulated XANES spectra, such as the white line and the second peak, around 10 eV above, are observed in the experimental spectrum, the second peak only as a shoulder in the data of the thin-film material. For a single-crystalline sample (not shown here) the second peak is more pronounced. The wiping out of the structure in the case of the Ge-implanted thin film may be the result of a higher local concentration in the implanted region. Similar to the EXAFS region, a distinction between the two different cationic positions is not possible. The different FMS XANES spectrum for an anionic Ge doping position excludes Ge_{Se} as a possible lattice site for Ge.

Another possible alternative could be an interstitial position as a result of the implantation process. As a test for such a position we placed the Ge on a position $(0.5a, 0.5b, 0.25c)$ and calculated the FMS XANES. The result is included in Fig. 3. The almost triangular shape of the white line with a slow fall-off toward higher energies seems to exclude the interstitial position. More convincing is the failure to fit the EXAFS spectrum with such an assumed interstitial position (see Fig. 2), for which the first-shell fit appears to be acceptable, but the structures at larger R are not reproduced and the K-edge energy E_0 turned out to be not realistic. Since an easy distinction between the two possible cationic substitutional lattice positions are not provided by the x-ray absorption data discussed here, a closer inspection is necessary.

B. Theoretical results and comparison with experiment

The ternary chalcopyrite-type crystal structure with the chemical formula I-III-VI_2 such as $CuGaSe_2$ (space group $I\bar{4}2d$ No.122) is similar to the monoelemental diamond and to the binary sphalerite (GaAs, e.g.) crystal structure. The sphalerite structure is characterized by metallic cations tetrahedrally coordinated by four anions, and vice versa, due to a strong sp^3 covalent-bonding interaction accompanying the ionic-bonding interaction between the group III cations and the group V anions. By maintaining this tetrahedral coordination and the corresponding sp^3 hybridization, the chalcopyrite unit cell can be derived from the sphalerite unit cell, when the group I and group III metallic cations (Cu^{1+} and Ga^{3+}, e.g.) are positioned at the cationic sites and the sphalerite unit cell is doubled. As a consequence of the different bonding strength between Cu^+ and Ga^{3+} with the Se^{2-} anions, the I-VI and III-VI bond lengths as labeled $R_{\text{Cu-Se}}$ and $R_{\text{Ga-Se}}$, respectively, are different. A consequence is the tetragonal distortion characterized by the quantity u as given by $u=\frac{1}{4}+\frac{R^2_{\text{Ga-Se}}-R^2_{\text{Cu-Se}}}{a_o}$ and the deformation characterized by the parameter $\eta=c/2a_o$. The parameter u describes the deviation of the Se^{2-} anions in the x-y plane of the unit cell from the ideal position of $\frac{1}{4}$ in the sphalerite structure[19] with a_o being the lattice constant in the x and y direction while η gives the deviation of the unit cell length in z direction c from $2a_o$. The corresponding bond lengths are related to these parameters by the equations

$$R_{\text{Cu-Se}} = a_o\sqrt{u^2+\frac{(1+\eta^2)}{16}}$$

and

$$R_{\text{Ga-Se}} = a_o\sqrt{\left(u-\frac{1}{2}\right)^2+\frac{(1+\eta^2)}{16}}.$$

The lattice parameters are taken from a very recent x-ray diffraction work[20] and an inorganic crystal-structure database (ICSD),[21] and the corresponding bond-length distances, $R_{\text{Cu-Se}}$ and $R_{\text{Ga-Se}}$ were calculated (see Table II). While the extracted lengths, as determined locally from our EXAFS data, are generally in agreement with the XRD data, the general trend of a smaller Ga-to-Se bond length compared to the Cu-to-Se bond length as observed in the XRD experiments due to a smaller Ga^{3+} ionic radius is barely found in our EXAFS analysis.

Starting from the conventional unit cell of $CuGaSe_2$ by using the calculated structural parameters, a supercell consisting of 64 atoms was constructed where one host cation was replaced by a Ge atom, which effectively corresponds to an impurity concentration of ~1.6 at. %. Two different charge-state situations were considered: (i) the neutral dopant Ge^0_{Ga} and Ge^0_{Cu} point defects and (ii) the two possible donorlike charged Ge^{1+}_{Ga} and Ge^{3+}_{Cu} point defects. The charged supercells are calculated by compensating the extra positive donor charge with a negative background charge smeared out over the complete supercell. The results of the theoretical lattice relaxation are summarized in Table III.

The local atomic lattice relaxation was found to be highly sensitive to the charge state of the point defect. Compared to the pure, undoped host lattice, we observe an expansion in

TABLE III. Calculated bond lengths around Ge in $CuGaSe_2$ to be compared with the value for the pure system of 2.441(2) and 2.394(2) Å for $R_{Cu\text{-}Se}$ and $R_{Ga\text{-}Se}$ from the recent XRD data (Ref. 18).

	Ge^{0}_{Ga}	Ge^{0}_{Cu}	Ge^{1+}_{Ga}	Ge^{3+}_{Cu}
R_{NN} (Å)	2.525	2.661	2.444	2.479

the first NN shell for all considered doping situations. Especially, the selenium NN shell exhibits a pronounced expansion for neutral Ge dopants occupying the Cu lattice position while only a small expansion was found for positively charged Ge^{1+} donors occupying the Ga lattice position. In general, the experimentally determined bond length in EXAFS in similar systems such as the tetrahedrally coordinated semiconductors, such as Si or II-VI compounds such as CdTe, is reasonably well matched by theory, like here with the LAPW calculations, with such a treatment of the extra charge Refs. 22–24. Therefore, one is tempted to take the only fair agreement in the case of the Ge^{1+} donor occupying the Ga lattice position as evidence for our assignment.

For further supporting our assignment, we now consider calculated electron density of states (DOS). Figure 4 compares the total (top set) and projected (bottom set) electron DOS of the charged Ge point doping defects, such as Ge-on-Ga (left side) and Ge-on-Cu (right side) in $CuGaSe_2$. The zero of the energy axis is set to the valence-band maximum, E_{VBM}, in the system. In the undoped $CuGaSe_2$ system, the valence band occurs between E_{VBM} and $E_{VBM}-6$ eV and exhibits two main groups: the deeper one is due to the bonding of Cu 3*d* to Se 4*p* and the upper one corresponds to the antibonding Cu 3*d*-Se 4*p* states. Deeper in the valence band, the Ga 4*s*-Se 4*p* bonding states are found below $E_{VBM}-7$ eV. The conduction band consists of Ga 4*s*-Se 4*p* antibonding states located at around $E_{VBM}+2$ eV. The calculated DOS here is in very good agreement with recent published data by Persson *et al.*[14] In both cases the total DOS of the doped $CuGaSe_2$ is similar to that of the undoped $CuGaSe_2$ system (not shown here) and the significant differences between the two doping situations can be discussed in more detail on the basis of the partial DOS as given in the bottom part of the Fig. 4. We observe two sharp and localized features with mostly Ge 4*s* character appearing in the band gap at $E_{VBM}+0.4$ eV for the Ge^{1+}_{Ga} point-defect system or directly at E_{VBM} for the Ge^{3+}_{Cu} point-defect system. In the valence band, two additional sharp and localized peaks appear at $E_{VBM}-8.8$ eV for Ge^{1+}_{Ga} and at $E_{VBM}-9.3$ eV for Ge^{3+}_{Cu}. One can also find *all* these bands in the total DOS *and* in the projected Se 4*s*- and Se 4*p*-related DOS (not shown here; the projected Se 4*p*-related DOS is dominating) with a substantial overlap of Se 4*p* orbitals at the same energy which strongly indicates that a sp^3 hybridization of Ge 4*s* and Se 4*p* orbitals occurs for both Ge point-defect systems. Hence, the dominant features in the band gap can be assigned to an antibonding Ge-Se $4sp^3$ defect band while the corresponding bonding states occur in the valence band at $E_{VBM}-8.8$ eV and $E_{VBM}-9.3$ eV. The antibonding Ge-Se $4sp^3$ related defect band in the Ge^{1+}_{Ga} point defect system is well above E_{VBM}, i.e., this defect band is unoccupied, while this band is directly at E_{VBM} in the Ge^{3+}_{Cu} point-defect system, i.e., this antibonding band is mostly occupied and the actual charge state here is +0.5, resulting from integrating over the unoccupied DOS. This strongly suggests that the Ge-to-Se-bonding strength is lowered due to an electron occupation of the antibonding Ge-Se $4sp^3$ related defect band in the case of the Ge^{3+}_{Cu} point-defect system which is not the case for the Ge^{1+}_{Ga} point-defect system. Hence, the Ge^{3+}_{Cu} point-defect system can be assigned to an almost filled acceptorlike defect band while the antibonding Ge-Se $4sp^3$ related defect band in the Ge^{1+}_{Ga} point-defect system can be attributed to an unoccupied donorlike electronic defect band.

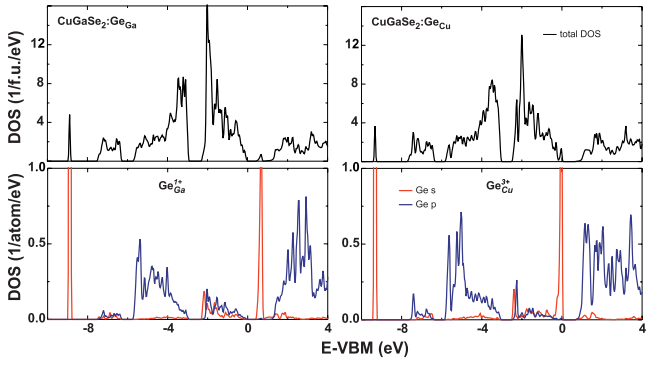

FIG. 4. (Color) Total electron density of states (DOS) of charged Ge dopants at cationic sites in $CuGaSe_2$:Ge_{Ga} (left) and Ge_{Cu} (right). The corresponding projected *s*- and *p*-related DOS are given at the bottom.

The overall shape of the DOS remains almost unchanged for the neutral doping system (not shown). For the neutral $CuGaSe_2$:Ge^{0}_{Cu} point-defect doping system, the Fermi level lies within the conduction band due to the additional electrons from the Ge doping atom. In this case the three additional electrons per Ge atom almost fill up the unoccupied bands at the bottom of the conduction band which can be attributed to a shallow donor defect band in the doped neutral system.

In the case of the neutral $CuGaSe_2$:Ge^{0}_{Ga} point-defect doping system the additional electrons occupy the new, unoccupied sharp Ge-related Ge-Se $4sp^3$ defect band located within the band gap and the Fermi level is at the top of this sharp defect band. Our theoretical band-structure model predicts the existence of additional localized acceptor and donor defect bands in the band gap of CGS originating from a strong covalent interaction between Ge 4*s* and Se 4*p* orbitals for Ge atoms tetrahedrally surrounded by Se nearest-neighbor atoms. Such a covalent-bonding configuration is forced by the locally tetrahedral symmetry of the Ga or Cu atoms surrounded by four Se nearest-neighbor atoms in the chalcopyrite unit cell. Indeed, such defect bands are observed in Ge ion-implanted thin films of $CuGaSe_2$. Especially, the newly observed DAP transition has to be attributed to a deep Ge-induced donor band in the near-surface doping region of the thin film, as shown in Fig. 1.

Hence, the theoretical evidence found here is in accordance with the appearance and the origin of the new Ge-dopant-related DAP transition. For the Ge^{1+}_{Ga} point-defect system the observed antibonding Ge-Se $4sp^3$ related defect band

appears well above the valence-band maximum at E_{VBM} $+0.6(\pm 0.1)$ eV (see Fig. 4, left bottom), this state can be assigned to the Ge-dopant-related donor. The new Ge-Se $4sp^3$ related donor defect band occurs well above the valence-band maximum, E_{VBM}, in the band-structure model at about $0.6(\pm 0.1)$ eV below the conduction band minimum (CBM). With respect to the energetic position of this new donor defect band, there is still a lack in the correct prediction by using the LDA model, which is very well known in the literature and is discussed in great detail by Persson *et al.*, e.g., (see the paragraph "LDA energy gap error" in the appendix of Ref. 14). Hence, we can here only qualitatively correlate the detected Ge-dopant-related new DAP emission at 1.47 eV as observed in Fig. 1 (for more details see Refs. 4 and 5), to an electron transition from the new Ge-Se $4sp^3$ related donor defect band into the copper vacancy-related acceptor defect band in the band gap of $CuGaSe_2$ chalcopyrite (see Refs. 6 and 7, e.g.).

On the basis of our theoretical results and by considering the recently found Ge-dopant-related DAP transition, we can conclude that (i) the most favored point-defect position of the Ge dopants is the cationic Ga site in $CuGaSe_2$ host lattice; (ii) the Ge atoms act most likely as donors; and (iii) the charged Ge_{Ga}^{1+} point-defect system is favored due to the appearance of a sharp, antibonding Ge-Se $4sp^3$ related defect band with high DOS well above the Fermi level within the band gap. This is supported by considering that the ionization energy of the +1 state (Ge^{1+}:+7.9 eV) is four times smaller if compared to the +3 state (+34.2 eV for Ge^{3+}) for atomic ions.[25] By taking into account that the point-defect formation energy of a copper vacancy, V_{Cu}^-, in wider-band-gap $CuGaSe_2$ is almost zero (from the recent literature, see Refs. 6 and 7, e.g.), the formation of electrically neutral donor-acceptor point-defect pairs of $[Ge_{Ga}^{1+}+V_{Cu}^-]$ is postulated here as a consequence of the doping. In a recent publication on *n*-type doping of $CuGaSe_2$, it has theoretically been predicted that the formation energy of a Cu vacancy is lowered as the Fermi energy moves toward the CBM.[14] Once the Fermi level crosses a certain point in the band gap where this formation energy for Cu vacancies becomes zero, the Cu atoms leave the lattice spontaneously. Since Cu vacancies are acceptors which capture free electrons, the Fermi level can no longer rise toward the CBM and is pinned at a certain point. In this case, donor doping is overcompensated by the electron accepting Cu vacancies formed spontaneously by *n*-type doping with Ge atoms. Thus, it is not possible to shift E_F to higher values toward the CBM under equilibrium conditions due to the nearly zero formation energy of the compensating V_{Cu} acceptors in $CuGaSe_2$.

Our theoretical model gives a hint toward *n* doping of $CuGaSe_2$ by considering that the Ge atoms occupy Ga lattice sites and the new antibonding Ge-Se $4sp^3$ donor defect band of the Ge_{Ga}^{1+} point-defect system is found to be well above the Fermi level. On the other hand, the high binding energy of ~ 0.6 eV below the CBM of this sharp and energetically separated antibonding donor defect band excludes *n*-type conductivity. The corresponding temperature-dependent Hall measurements performed on $CuGaSe_2$ thin films with implanted Ge ions show that the doped thin films are electrically compensated and do not give any unequivocal evidence for a *n* conductivity. This has also been found for single-crystalline CGS doped with about 0.1–0.3 at. % Ge. Hence, this may explain that the presented attempts of an *n*-type doping under nonequilibrium ion-implantation conditions were not successful, too.

V. CONCLUSIONS

The local atomic structure around the Ge dopants in chalcopyrite $CuGaSe_2$:Ge was studied by using EXAFS spectroscopy. We have found that Ge dopants substitute the cation positions of Cu or Ga in the chalcopyrite host lattice $CuGaSe_2$:Ge but that EXAFS cannot distinguish between a Ge_{Ga}^{1+} or a Ge_{Cu}^{3+} point defect. The theoretically calculated bond distances of Ge_{Cu}-Se and Ge_{Ga}-Se give an indication for a Ga site preference. Theoretical evidence was found here for the appearance of a new Ge-dopant-related DAP transition in the corresponding photoluminescence spectra. Our band-structure model predicts the existence of additional localized electronic acceptor and donor defect bands in the band gap of $CuGaSe_2$ originating from a strong covalent interaction between Ge 4*s* and Se 4*p* orbitals for Ge atoms tetrahedrally bonded by four Se nearest-neighbor atoms. Such a covalent-bonding configuration is forced by the local tetrahedral symmetry of the Ga or Cu atoms surrounded by Se nearest-neighbor atoms in the chalcopyrite unit cell. A new antibonding Ge-Se $4sp^3$ related defect band observed for the Ge_{Ga}^{1+} point-defect system appears well above the valence-band maximum, E_{VBM}, in the band gap and can be attributed to a donor defect band as experimentally found in our recent PL study. The new Ge-Se $4sp^3$ donor defect band exhibits a high DOS in the band-structure model, it is deeply located within the band gap at about $0.6(\pm 0.1)$ eV above the valence-band maximum, E_{VBM}, and it is well separated from the conduction band [about $0.6(\pm 0.1)$ eV below the CBM]. Hence, we can exclude the *n*-type conductivity of the $CuGaSe_2$:Ge doping system due to this large energetic separation from the CBM. Furthermore, by taking into account that the point-defect formation energy of a copper vacancy, V_{Cu}^-, in wider-band-gap $CuGaSe_2$ is almost zero, the formation of an electrically neutral donor-acceptor point-defect pair of $[Ge_{Ga}^{1+}+V_{Cu}^-]$ is postulated here as a consequence of the doping. We finish our conclusion with the outlook that the Ge-doped $CuGaSe_2$ semiconducting compound is a potential candidate for the theoretically postulated so-called *intermediate band material* due to the Ge-dopant induced formation of a sharp, well-separated donor state with a high DOS in the chalcopyrite band gap.[26]

ACKNOWLEDGMENTS

This work was supported by Deutscher Akademischer Austauschdienst (DAAD) via the PhD stipendiary program (Serge Doka-Yamigno from Cameroon). Two authors (S.D.-Y. and Th. S.-N.) are very much obliged to Sven Wiesner for the thin-film preparation by means of the CCSVT technique and to Norbert Fabre *et al.* from LAASS-CNRS in Toulouse for performing the Ge implantation. We

acknowledge the Hamburger Synchrotronstrahlungslabor (HASYLAB) at Deutsches Elektronen-Synchrotron (DESY) for providing beamtime at their synchrotron radiation facilities, and the authors are grateful, especially to E. Welter and the HASYLAB staff at DESY for his and their assistance at the A1 beamline. V.K. would like to acknowledge the help from the Serbian Ministry of Science under the Grant No. 141022G.

*Corresponding author.

†Also at Freie Universität Berlin, Fachbereich Physik, Arnimallee 14, D-14195 Berlin, Germany.

[1] I. Repins, M. A. Contreras, B. Egaas, C. DeHart, J. Scharf, C. L. Perkins, B. To, and R. Noufi, Prog. Photovoltaics **16**, 235 (2008).

[2] J. H. Schön, E. Arushanov, L. L. Kulyuk, A. Micu, D. Shaban, V. Tezlevan, N. Fabre, and E. Bucher, J. Appl. Phys. **84**, 1274 (1998).

[3] J. Krustok, J. Raudoja, and J. H. Schön, Phys. Status Solidi A **178**, 805 (2000).

[4] S. Doka, M. Rusu, A. Meeder, E. Arushanov, N. Fabre, S. Fiechter, Th. Schedel-Niedrig, and M. Ch. Lux-Steiner, *Thin-Film Compound Semiconductor Photovoltaics*, MRS Symposia Proceedings Vol. 865 (Materials Research Society, Pittsburgh, 2005), p. F5.27.1.

[5] S. Doka-Yamigno, Ph.D. thesis, Freie Universität Berlin, 2006.

[6] A. Zunger, Appl. Phys. Lett. **83**, 57 (2003).

[7] Y.-J. Zhao, C. Persson, S. Lany, and A. Zunger, Appl. Phys. Lett. **85**, 5860 (2004).

[8] P. Blaha, K. Schwarz, G. Madsen, D. Kvasnicka, and J. Luitz, in *WIEN2k: An Augmented Plane Wave Plus Local Orbitals Program for Calculating Crystal Properties*, edited by K. Schwarz (Technische Universität Wien, Austria, 2001).

[9] M. Rusu, S. Wiesner, D. Fuertes Marrón, A. Meeder, S. Doka, W. Bohne, S. Lindner, Th. Schedel-Niedrig, Ch. Giesen, M. Heuken, M. Ch. Lux-Steiner, Thin Solid Films **451-452**, 556 (2004).

[10] M. Rusu, S. Doka, C. A. Kaufmann, N. Grigorieva, Th. Schedel-Niedrig, and M. Ch. Lux-Steiner, Thin Solid Films **480-481**, 341 (2005).

[11] R. Würz, A. Meeder, D. Fuertes Marrón, Th. Schedel-Niedrig, A. Knop-Gericke, and K. Lips, Phys. Rev. B **70**, 205321 (2004); R. Würz, M. Rusu, Th. Schedel-Niedrig, M.Ch. Lux-Steiner, H. Bluhm, M. Hävecker, E. Kleimenov, A. Knop-Gericke, and R. Schlögl, Surf. Sci. **580**, 80 (2005).

[12] J. Hofstetter, Diploma thesis, Freie Universität Berlin, 2006.

[13] P. Perdew, K. Burke, and M. Ernzerhof, Phys. Rev. Lett. **77**, 3865 (1996).

[14] C. Persson, Y.-J. Zhao, S. Lany, and A. Zunger, Phys. Rev. B **72**, 035211 (2005).

[15] A. Bauknecht, S. Siebentritt, J. Albert, and M. Ch. Lux-Steiner, J. Appl. Phys. **89**, 4391 (2001).

[16] J. I. Pankove, *Optical Processes in Semiconductors* (Cambridge University Press, Cambridge, 1991).

[17] B. Ravel and M. Newville, J. Synchrotron Radiat. **12**, 537 (2005).

[18] A. L. Ankudinov, B. Ravel, J. J. Rehr, and S. D. Conradson, Phys. Rev. B **58**, 7565 (1998).

[19] J. E. Jaffe and A. Zunger, Phys. Rev. B **29**, 1882 (1984).

[20] S. Lehmann, Ph.D. thesis, Freie Universität Berlin, 2007.

[21] Inorganic crystal structure database, http://www.fiz.karlsruhe.de/ecid/Internet/de/DB/icsd/index.html

[22] V. Koteski, N. Ivanović, H. Haas, E. Holub-Krappe, and H.-E. Mahnke, Nucl. Instrum. Methods Phys. Res. B **200**, 60 (2003).

[23] V. Koteski, H. Haas, E. Holub-Krappe, N. Ivanović, and H.-E. Mahnke, J. Alloys Compd. **371**, 138 (2004).

[24] H.-E. Mahnke, H. Haas, E. Holub-Krappe, V. Koteski, N. Novaković, P. Fochuk, and O. Panchuk, Thin Solid Films **480-481**, 279 (2005).

[25] *CRC Handbook of Chemistry and Physics*, 82nd ed. (CRC Press, Cleveland/Boca Raton, 2001), p. 10–175.

[26] A. Luque and A. Marti, Phys. Rev. Lett. **78**, 5014 (1997).